Metal-nanoshelled three-dimensional photonic lattices

Koshiro Kaneko,[1] Kazuo Yamamoto,[1] Satoshi Kawata,[1] Hong Xia,[2] Jun-Feng Song,[2] and Hong-Bo Sun[2],*

[1]*Department of Applied Physics, Osaka University, Suita, Osaka 565-0872, Japan*
[2]*State Key Laboratory on Integrated Optoelectronics, College of Electronic Science and Engineering,
Jilin University, 2699 Qianjin Street, Changchun 130012, China*
*Corresponding author: hbsun@jlu.edu.cn

Micronanostructures prepared by two-photon photopolymerization are utilized as templates for electroless plating of metals, giving rise to an approach for fabricating complex-shaped metal micronanostructures that are so far not achievable by other means. We show that when the coated-layer thickness of a metal coating is larger than a critical value (around 20 nm for silver at $2-3$ μm wavelength) associated with the metal's skin depth, the photonic crystals exhibit optical properties more comparable to a solid metal structure than to their polymer counterparts. © 2008 Optical Society of America
    OCIS codes: 140.3390, 160.3900.

Over the past several years there has been growing interest in corrugated metallic thin films and metal nanostructures, owing to the rebirth of the concept of surface plasmonics [1–6]. Enormous investigations have been carried out on transmission enhancement through subwavelength arrays of holes [1], creation of metamaterials with permeability and permittivity simultaneously negative [2,3], Raman scattering enhancement aimed at biosensing [4], and high-resolution, near-field detection with a metallic tip [5,6]. Most structures attained so far are of zero, one, or two dimensions. Very few experiments have been conducted to describe 3D metal micro-nanostructures, despite the fact that unique electromagnetic properties have been theoretically expected [7–10]. The underlying reason for this is in that the realization of 3D metallic structures is technically challenging. In this Letter, we solve this problem by combining laser micronanofabrication technology [11,12] with surface-metal coating. The desired 3D photonic crystals (PhC) structures are first templated via two-photon photopolymerization, and then the polymer PhC skeletons were homogeneously coated with metal. It has been found that when the metal layer becomes thicker than a critical value, the structure behaves the same as pure metal structures, as theoretically predicted [7].

Several approaches have been tried to produce a metallic thin layer on polymer microstructures. Figure 1(a) shows a two-photon polymerized microbull sculpture coated by means of thermal evaporation of silver. Although high surface quality has been observed on the top side of the bull, the belly of the bull remains bare regardless of the duration of evaporation. As an alternative solution, we turned to electroless plating [13,14], for which the technical route is illustrated in Figs. 1(b) and 1(c). A polymer micronanostructure that was laser written onto a glass substrate, in this case, a diamond-lattice PhC [15] [inset of Fig. 1(b)], was first immersed in a $SnCl_2$ solution for surface affinity modification. The reducing agent of Sn^{2+} was uniformly absorbed and covered the polymer surface [Fig. 1(b)]. Next, the structure was set in an ammoniac $AgNO_3$ bath wherein a redox reaction occurs involving the oxidation of surface Sn^{2+} to Sn^{4+} and reduction of Ag^+ to Ag^0 [the inset of Fig. 1(c)]. In order for the silver deposition to proceed after the exhaustion of the surface reductant Sn^{2+}, potassium sodium tartrate tetrahydrate $(C_4H_4KNaO_6\cdot4H_2O)$ was mixed with the metal salt solution as an additional reductant. The early formed silver film acts as catalyst to ensure that the ensuing reduction continues only at the existing silver surface. Experimentally, 1 g $AgNO_3$ was dissolved into 50 ml pure water, to which 2.25 ml 28% ammonia solution was gradually added. The mixture was observed roiling, first presenting white-brown color,
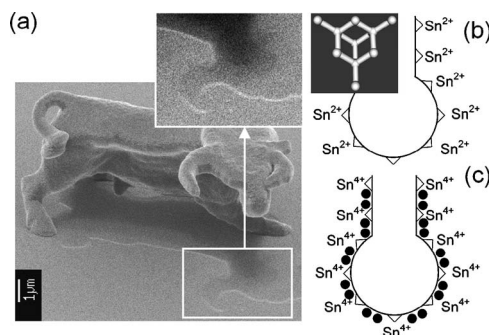
Fig. 1.   Metal coating of polymer templates. (a) SEM image of a microbull sculpture coated by thermal evaporation of silver. The polymer microbull as template was formed by two-photon photopolymerization of resin (SCR500, JSR) with laser pulses of 130 fs width, 780 nm wavelength, and 82 MHz repetition rate. The laser beam was focused by a high NA ($\sim$1.4) objective lens and exposed the resin point by point by translating a 3D piezoelectric sample stage according to a programmed pattern under computer control. The shadow under the bull indicates the invalidity of this method owing to the straight-line projection of thermal atoms. (b) Surface-affinity modification for electroless plating, by which a complete metal layer covering the entire target structure is expected. The inset is an illustrative PhC template unit. (c) Silver atoms (denoted by ●) plating by a redox reaction.

and then turning transparent. A solution of 5 g potassium sodium tartrate dissolved in 50 ml pure water was mixed with the $[Ag(NH_3)]^{2+}$ complex solution as the plating bath. Polymer surface modification was conducted in a solution of 0.49 g $SnCl_2$ in 100 ml pure water. A 4.2 nm/min growth rate, enabled by the slow exhaustion of the bath solution, was measured, indicating the possibility of nanometer-order thickness control.

Figures 2(a) and 2(b) show a plated microhand and a microbull with a silver thickness of 41 nm, both with satisfactory roughness. Further investigation of these apparently smooth surfaces by atomic force microscopy found that they consist of particles of 20 nm average diameter. This affects the optical properties of the surface significantly, for instance, the 317 nm transmission peaks in Fig. 2(c), measured from a flat polymer surface plated simultaneously, are the finger feature of the plasma resonant absorption, λ_P, for thin but still closed silver films consisting of particles. With increasing detection wavelength, moving away from λ_P, the transmission gradually falls to a critical value λ_C, which is dependent on skin depth, δ. δ is an index of how thick an electromagnetic wave can penetrate a metal before the amplitude of the electric field is reduced to $1/e$. δ is defined as $\delta = \sqrt{2/\omega\mu\sigma}$, where ω is the angular frequency of light, μ is the absolute magnetic permeability, and σ is the electric conductivity. For silver, $\sigma = 6.1 \times 10^7$ S/m and $\mu = 4\pi \times 10^{-7}$ H/m, giving rise to $\delta = 2.6$ nm and 5.5 nm for 600 nm and 2.7 μm wavelengths, respectively. Experimentally the light may penetrate deeper owing to the looser packing of particles. The transmission rises after λ_C indicates that the skin depth for wavelengths of $>\lambda_C$ is not larger than the film thickness, for example, $\delta \leqslant 23$ nm for $\lambda = 600$ nm [Fig. 2(c)]. According to the square root law, we should have $\delta \leqslant 49$ nm for $\lambda = 2.7$ μm light. However, no similar transmission valley appears for thicker films, i.e., 55 and 66 nm even if the observation has been extended to the infrared region, 6 μm [Fig. 2(d)]. A deeper insight into the wavelength dependence of the skin depth in the optical range will be an immediate task of future study.

The nature of slow surface chemical reactions makes electroless plating applicable to more complicated structures like PhC (Fig. 3). Even with an abundance of deliberately high aspect ratio structures, a homogeneous coated layer of metal was found from the exterior into the core portions of the structure, as measured by a layer-by layer cutting by a focused ion beam (FIB). After immersion of the surface-opened PhCs in ethanol for several hours, the polymer template, as long as it has no history of further exposure after its creation, is removed, leaving a metal PhC shell [Fig. 3(a)]. The fingerprint of the bandgap effect effects are confirmed by a numerical calculation and by the complementary shape in the reflection and transmission spectra peaking at 3550 cm^{-1} from the polymer template [Fig. 3(b)]. Consequently, it is natural to explore the dependence of bandgap effects on the metal thickness, including the spectral broadening, owing to the existence of skin depth phenomena as discussed on Figs. 2(c) and 2(d). PhC templates of identical structural parameters are coated with varied thicknesses of 14, 20, 23, 27, 40, 55, and 66 nm, all possessing high surface quality, judging from magnified scanning SEM images [Fig. 4(a) and insets there]. It is interesting to note from the series of reflection spectra that there seems to exist a critical thickness, Δ_c near 23 nm.
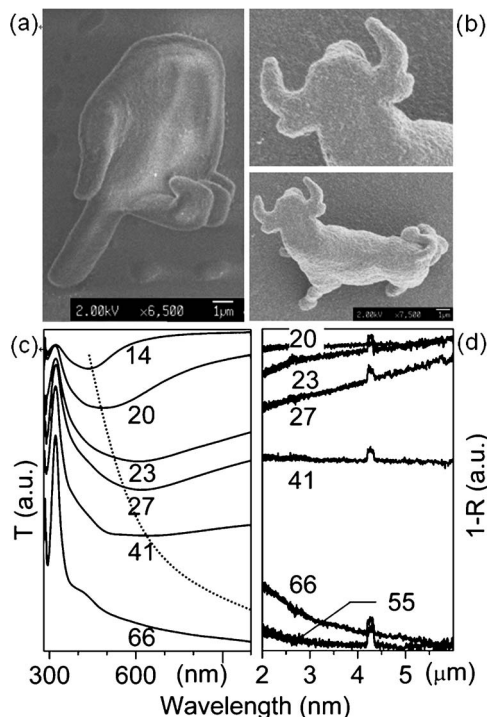
Fig. 2. Electroless plated structures and properties of metal thin films. (a) A microhand, and (b) a microbull; both are obtained with satisfying surface quality. (c) and (d) are the transmissions of the thin film coatings of different thicknesses in the visible and IR wave ranges, respectively. For the convenience of comparison, the latter is presented as 1-R. The dashed curve indicates the tendency of skin depth to increase with increasing wavelength.
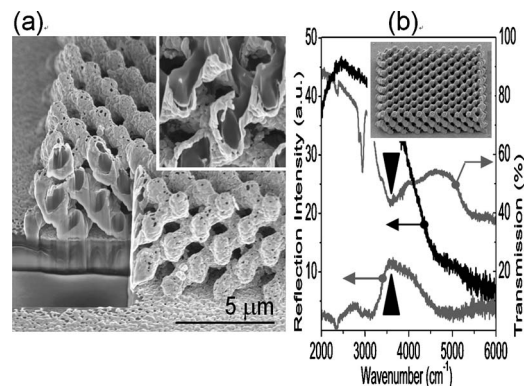
Fig. 3. Silver-nanoshelled photonic lattices and their characteristics. (a) A scanning electron microscopy (SEM) image of the top view of a diamond-lattice PhC, which was cut by FIB, and then the interior polymer was dissolved. The inset is a magnified view of the remaining metal shell. (b) FTIR reflection spectra of a coated PhC (black curve and inset). The gray curves are from a polymer PhC template as reference. The arrows point to the region where a photonic-bandgap effect occurs.
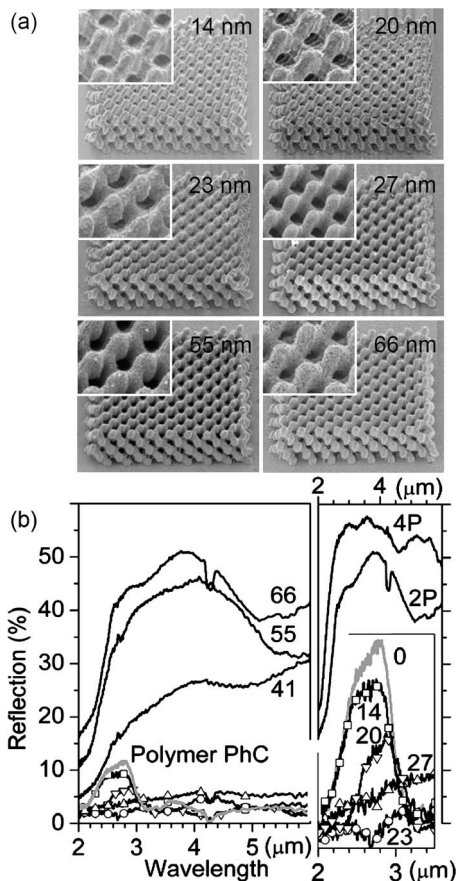
Fig. 4.   Metal-nanoshelled photonic lattices of different thickness of silver layers. (a) SEM images of plated structures. The insets show a locally magnified view. (b) Reflection spectra from two-period (left) and four-period (right) structures. The reflections from structures of $\Delta < \Delta_c$ at short wavelengths are magnified in the inset at the right part of the figure.

When the silver thickness $\Delta < \Delta_c$, the intensity of the reflection peak gradually reduces as Δ increases, from 12% in a pure polymer PhC to near zero in the Δ_c-thick structure; see right lower inset of Fig. 4(b) for a better view. Further increasing Δ leads to a dramatic enhancement of the bandgap features, when $\Delta = 66$ nm, the half-width of the reflection band is over 10 times wider, and the peak is more than four times stronger, with its intensity tending to saturate at 50% reflection. Larger enhancement has been further achieved from thicker samples, as shown by the four-period PhC [right part of Fig. 4(b)]. The physics behind this phenomenon may be very simply described. When $\Delta < \Delta_c$, (a) light penetrates the polymer core, undergoing multiple transmissions and reflections between air–metal–polymer interfaces; and (b) absorption and scattering loss caused by the compositional nanoparticles could be enhanced by increase of the amount of metal. When the thickness becomes larger than Δ_c, the factors causing the reflection power loss are saturated, while the photonic bandgap effects begin to dominate [16]. Comprehensively determined by enhancement factor of the photonic bandgap effect, and such power loss factors as scattering and metal absorption, Δ_c is not equal to the skin depth itself (the case of flat metal films), but closely related to it. Owing to the skin depth, the polymer core becomes insignificant to the incident electromagnetic wave upon $\Delta > \Delta_c$, and the coated PhCs behave the same as pure metal PhCs [Fig. 4(b)] [17].

In summary, the combination of two-photon polymerization and electroless plating results in an practical approach for arbitrarily designed 3D metal-nanoshelled photonic lattices and other complicated micronanostructures. They exhibit performance similar to those of pure metal PhCs when the coating thickness is larger than a critical value. Such metal structures, potentially possessing a full plasmonic/photonic bandgap, may find important applications in blackbody emission control, left-handed materials, and terahertz-wave generation and manipulation.

References

1. T. W. Ebbesen, H. J. Lezec, H. F. Ghaemi, T. Thio, and P. A. Wolff, Nature **391**, 667 (1998).
2. V. G. Veselago, Sov. Phys. Solid State **8**, 2854 (1967).
3. J. B. Pendry, Phys. Rev. Lett. **85**, 3966 (2000).
4. W. L. Barnes, A. Dereux, and T. W. Ebbesen, Nature **424**, 824 (2003).
5. Y. Inouye and S. Kawata, Opt. Lett. **19**, 159 (1994).
6. T. Ichimura, N. Hayazawa, M. Hashimoto, Y. Inouye, and S. Kawata, Phys. Rev. Lett. **92**, 220801 (2004).
7. A. Moroz, Phys. Rev. Lett. **83**, 5274 (1999).
8. A. L. Pokrovsky and A. L. Efros, Phys. Rev. Lett. **89**, 093901 (2002).
9. J. Li, G. Sun, and C. T. Chan, Phys. Rev. B **73**, 075117 (2006).
10. A. V. Akimov, A. A. Meluchev, D. A. Kurdyukov, A. V. Scherbakov, A. Holst, and V. G. Golubev, Appl. Phys. Lett. **90**, 171108 (2007).
11. H. B. Sun, S. Matsuo, and H. Misawa, Appl. Phys. Lett. **74**, 786 (1999).
12. S. Kawata, H.-B. Sun, T. Tanaka, and K. Takada, Nature **412**, 697 (2001).
13. P. Andrew and W. L. Barnes, Science **206**, 1002 (2004).
14. Z. Chen, P. Zhan, Z. L. Wang, J. H. Zhang, W. Y. Zhang, N. B. Ming, C. T. Chan, and P. Sheng, Adv. Mater. (Weinheim, Ger.) **16**, 417 (2004).
15. K. Kaneko, H. B. Sun, X. M. Duan, and S. Kawata, Appl. Phys. Lett. **83**, 2091 (2003).
16. A. Moroz, Phys. Rev. B **66**, 115109 (2002).
17. J. G. Fleming, S. Y. Lin, I. El-Kady, R. Biswas, and K. M. Ho, Nature **417**, 52 (2000).